IEEE Access
Multidisciplinary | Rapid Review | Open Access Journal

Received May 2, 2018, accepted June 14, 2018, date of publication June 21, 2018, date of current version July 12, 2018.

Digital Object Identifier 10.1109/ACCESS.2018.2849412

Optimization of Dual Frequency-Difference MIT Sensor Array Based on Sensitivity and Resolution Analysis

CHAO TAN, (Senior Member, IEEE), YIRAN WU, ZHILI XIAO, AND FENG DONG, (Senior Member, IEEE)

Tianjin Key Laboratory of Process Measurement and Control, School of Electrical and Information Engineering, Tianjin University, Tianjin 300072, China

Corresponding author: Chao Tan (tanchao@tju.edu.cn)

This work was supported in part by the National Natural Science Foundation of China under Grant 61571321 and Grant 61611130126 and in part by the Natural Science Foundation of Tianjin City under Grant 16PTSYJC00060.

ABSTRACT Magnetic induction tomography (MIT) is a promising technology for intracranial hematomas imaging. The existing problems in MIT are mainly low sensitivity and low resolution of the sensor array, which is necessary to be optimized. A number of optimizations exist to enhance the resolution of MIT, but so far, studies only considered the eigenvalue or singular value of the sensitivity, or the magnetic flux with noise-free data or low level of noise. In this paper, the optimization considers the intensity and uniformity of the sensitivity matrix with added noise. In order to enhance the resolution of dual frequency-difference MIT, the coil parameters optimization is studied by simulations from three aspects: the inner radius, the shape, and the number of turns. After the sensitivity analysis, the absolute dimensions of the optimal coil structure are determined. Based on the optimal structure, the brain hematoma is simulated with a human brain model and finite element method. Images are reconstructed from the modeled data with a 26-dB signal-to-noise ratio noise contaminated. The results indicated that the optimal sensor array can achieve the conductivity resolution of 0.25 S/m and the spatial resolution is 12.38% of the brain radius.

INDEX TERMS Magnetic induction tomography, coil optimization, sensor array, intracranial hematoma, spatial resolution, conductivity resolution.

I. INTRODUCTION

Intracranial hematomas are caused by trauma, hypertension, blood disease or other factors, accompanied with symptoms such as disturbance of consciousness, which seriously damages human health [1]. The position and the size of the hematoma are vital to the diagnosis. Thus, there is an urgent need to develop a new medical imaging method for long-term dynamic monitoring of intracranial hematomas. In clinical diagnosis, medical imaging methods are mainly computed tomography (CT) and magnetic resonance imaging (MRI). However, these two methods are either radioactive or expensive [2]. And the equipment is also bulky and not portable. Therefore, they are not suitable for long-term and continuous dynamic monitoring [3].

Magnetic induction tomography (MIT) and electrical impedance tomography (EIT) are attractive techniques in biomedical continuous monitoring due to the non-radioactive, non-invasive, low cost and portable features [4], [5]. Compared to EIT, MIT is contactless and the magnetic field is more easily to penetrate the low conductivity skull and thus more suitable for continuous brain imaging than EIT. Many MIT approaches have been investigated to focus on imaging brain [6], lung [7], heart [8], liver [9] and biological tissues [10]. MIT applies a primary magnetic field from the exciting coil, then a secondary magnetic field is generated by the eddy current induced in the object which carries the conductivity distribution. By measuring this secondary field, the brain hematoma size and location will be reconstructed. However, the image resolution is generally low for electrical tomography due to the dispersed nature of the electromagnetic field [11]. MIT suffers from low resolutions in biological imaging because the effective signals of the secondary magnetic field induced in brain are weak. It is therefore difficult to separate the effective signals from the strong primary magnetic field.

To enhance the resolution, one effective approach is to optimize the sensor array to improve its sensitivity to the weak secondary magnetic field. Much research has been conducted to achieve this goal. Most of the systems use sensor array for detection instead of scanning the sensor mechanically, which

reduces the requirement for accurate and fast scanning [12]. Peyton *et al.* designed a 16-coil MIT system, each coil acted as an exciting coil and a sensing coil, which is a classic way of placing sensing coils and has been adopted in sensor design since then [13]. Scharfetter *et al.* developed an MIT system consisting of a sensor array with planar gradiometer that could cancel the primary magnetic field generated by the exciting coil [14]. Scharfetter *et al.* also analyzed several receiver designs with different coil orientations about reconstruction stability and resolution. The criterion of the analysis was the nonzero singular value [15]. Lv *et al.* studied the influence of the sensor array on measurements. The impact of the distance between the exciting coil and the sensing coil was studied. The parameters also included the amplitude and frequency of the exciting coil current. The impact of these parameters was based on the analysis of magnetic flux [16]. Xu *et al.* optimized the sensor array from four aspects: coils number, location, diameter and shape. Under various sensor models, the eigenvalue spectrum of every sensitivity matrix was calculated as the criterion [17]. Most of the research considered the coil optimization from one single criterion such as the nonzero singular value and the eigenvalue of the sensitivity matrix, which represent the amount of information that the sensitivity matrix can provide. These criteria are not comprehensive enough and the effects of the sensitivity matrices on imaging are not fully considered. In this study, both the intensity and the uniformity of the sensitivity matrix are considered in the coil optimization, which are directly related to the quality of the reconstructed images. The criteria of the optimization is more comprehensive than the former research.

To evaluate the coil optimization, the spatial resolution and conductivity resolution of the optimal sensor array are studied. The spatial resolution of an MIT system relies on the independent combinations of transmitters and receivers [18]. For a simulated 3D MIT system with square arrays of coils set by Gencer and Tek, the spatial resolution was 10% of the array width. The signal-to-noise ratio (SNR) was assumed to be 80dB [19]. For a 16-transceiver MIT system set by Korjenevsky *et al.*, the theoretical maximum spatial resolution was approximately 9% of the array diameter, which would be degraded by noise [20]. The conductivity resolution depends on the volume of the measured tissues and the level of noise [18]. Measurements of 2S/m saline solution were performed by Griffiths *et al.* at 10MHz when the noise level was $<10^{-4}$ radian. The results indicated that the conductivity resolution was 0.01S/m. However, the results were misleading because the baseline drifting was sometimes large which was equivalent to the conductivity change of 0.2S/m [18], [21]. Most of these resolution studies involve no noise or the level of noise is less than the practical situation. Therefore, the aim to provide good resolution of reconstructed images in MIT is still under investigation [22].

In this study, coil parameters are optimized to enhance MIT resolution based on numerical simulations. In the optimization, the sensitivity matrices are analyzed under different coil models. The optimal coil structure is described in absolute dimensions as the size of brain is relatively fixed. Based on the optimal sensor array, the reconstructed conductivity distribution is compared to the actual distribution to verify the optimization, where 26dB noises were added to test the robustness of the optimized coils. To evaluate the results of the optimization, the conductivity resolution and spatial resolution are obtained in the detection of intracranial hematomas by optimal coils.

II. MAGNETIC INDUCTION TOMOGRAPHY

MIT is based on the electromagnetic induction principle. In the measured field, the exciting coil generates a sinusoidal alternating primary magnetic field B. The eddy current induced in the medium with conductivity produces a secondary magnetic field ΔB. The superimposed magnetic field is expressed in the form of induced voltage V. The voltage at the sensing coil will be perturbed if the conductivity distribution in the measured field is changed. The perturbation is shown in the phase change $\Delta\Phi$ of V. In this study, $\Delta\Phi$ is calculated by frequency-difference method [23]. According to the frequency characteristics of biological tissues conductivity, 1MHz and 10MHz are chosen to include the dielectric dispersion of blood centred around 7MHz [24]. Based on the $\Delta\Phi$, the conductivity distribution is reconstructed.

A. FORWARD PROBLEM

The forward problem of MIT is the process of obtaining $\Delta\Phi$ from the conductivity distribution and the signal of exciting coils. The foundation for solving the forward problem is Maxwell equation group (1). The induced voltage of the sensing coil is calculated as (2).

$$\begin{cases} \nabla \times H = J_e + J_s \\ \nabla \times E = -j\omega B \\ \nabla \cdot B = 0 \\ \nabla \cdot D = 0 \end{cases} \tag{1}$$

$$V = -j\omega \oint A dl \tag{2}$$

where J_e is the eddy current density, J_s is the source current density, H is the magnetic field strength, E is the electric field intensity, B is the magnetic flux density, D is the electrical displacement vector, A is the magnetic vector potential.

According to the measurement method of MIT forward problem proposed by Scharfetter *et al.* [14], the calculation of $\Delta\Phi$ can be transformed into the calculation of the imaginary part of $\Delta V/V$. Therefore, $\Delta\Phi$ is computed by (4) with frequency-difference method.

$$\begin{cases} \Delta V_{f_1} = V_{f_1} - V_{f_1}^0 \\ \Delta V_{f_2} = V_{f_2} - V_{f_2}^0 \end{cases} \tag{3}$$

$$\Delta\Phi = \frac{f_2}{f_1}\mathrm{Im}\left(\frac{\Delta V_{f_1}}{V_{f_1}^0}\right) - \mathrm{Im}\left(\frac{\Delta V_{f_2}}{V_{f_2}^0}\right) \tag{4}$$

where V_{f_1} is the sensing coil voltage at the frequency of 1MHz, V_{f_2} is the voltage at the frequency of 10MHz, $V_{f_1}^0$ and $V_{f_2}^0$ are the primary voltages at the frequency of 1MHz and 10MHz respectively [25], [26].

The relationship between $\Delta\Phi$ and the conductivity change $\Delta\sigma$ can be expressed as (5):

$$S\Delta\sigma = \Delta\Phi \tag{5}$$

where S is the sensitivity matrix, which expresses the relationship between $\Delta\Phi$ and $\Delta\sigma$ in the measured field [20]. It can be computed as follows [26], [27]:

$$(S)_{m,i} = \frac{E^a|_i E^b|_i}{(V^0)_{a,b}} \Delta x^3 \tag{6}$$

where m is the combination of the exciting coil a and the sensing coil b, i is the number of voxels. $E^a|_i$ or $E^b|_i$ is the electric field intensity in voxel i when the exciting coil a or b is activated. $(V^0)_{a,b}$ is the primary voltage of the sensing coil b when the exciting coil a is activated. Δx is the side length of the voxel.

B. INVERSE PROBLEM

The inverse problem of MIT is to acquire the distribution of $\Delta\sigma$ from the excitation and $\Delta\Phi$, which is a non-linear and ill-conditioned problem [28]. $\Delta\sigma$ is unknown that needs to be solved and $\Delta\Phi$ is obtained from the forward problem. As S is not a square matrix, the inverse of S is unable to be obtained. Therefore, solving (5) needs the image reconstruction algorithm. In order to avoid reaching a conclusion by chance, three algorithms are selected in this study, namely Landweber iteration, Newton-Raphson method and Tikhonov regularization. Landweber iteration and Newton-Raphson method are iterative methods, whose idea is to compare the difference between the measured voltage and the calculated voltage. After the comparison, the distribution of the conductivity is modified constantly. When the difference is less than a certain value, the calculated conductivity is considered to be the actual distribution. The solution of Landweber iteration can be expressed as (7):

$$\begin{cases} \Delta\sigma_0 = 0 \\ \Delta\sigma_{k+1} = \sigma_k - \alpha S^T(S\Delta\sigma_k - \Delta\Phi) \end{cases} \tag{7}$$

where the relaxation factor α satisfies $0 < \alpha < 2/\beta_1^2$. β_1 is the largest singular value of S. Newton-Raphson method can be expressed as (8):

$$\begin{cases} \Delta\sigma_0 = 0 \\ \Delta\sigma_{k+1} = \sigma_k - (S^T S + \gamma I)S^T(S\Delta\sigma_k - \Delta\Phi) \end{cases} \tag{8}$$

where I is the identity matrix, γ is an appropriate positive decimal. As for the non-iterative method, the principle of regularization is to find a solution set constrained by prior information and then choose a solution. The solution of Tikhonov regularization method is expressed as (9):

$$\Delta\sigma = (S^T S + \lambda I)^{-1} S^T \Delta\Phi \tag{9}$$

where λ is the regularization factor. The quality of Tikhonov regularization method mainly depends on the choice of λ. A small λ may give a good approximation of the original problem, while the influence of the error may lead to unacceptable solution. A large λ reduces the sensitivity of the solution to the error, but the solution deviates too far from the true value. The factors of above algorithms are selected to obtain the best quality of the reconstructed images, so the optimization can be compared on a reliable ground.

C. SIMULATION MODEL AND OPTIMIZATION PARAMETERS

In this study, a three-dimensional brain model is set for simulations. As the real brain has complex structure and shape, the brain model with real distribution will greatly increase the complexity of finite element analysis. Therefore, a simplified brain model was usually considered in related studies. In the study of electroencephalogram (EEG) problems, the three-dimensional concentric spherical model was firstly used to approximate the brain model [29]. In this simulation, a four-layer concentric spherical model is established to simulate the brain. From outside to inside, four layers are respectively scalp, skull, cerebrospinal fluid (CSF) and brain. The dimensions and conductivities of each layer are shown in Table 1 [25].

TABLE 1. Parameters of brain model.

Tissues	Scalp	Skull	CSF	Brain	Blood
Relative radius (%)	100	94.67	86.67	84.00	14.29
Absolute Radius (mm)	105	99.40	91.00	88.20	15
Conductivity at 1MHz (S/m)	0.01	0.06	2.00	0.10	0.82

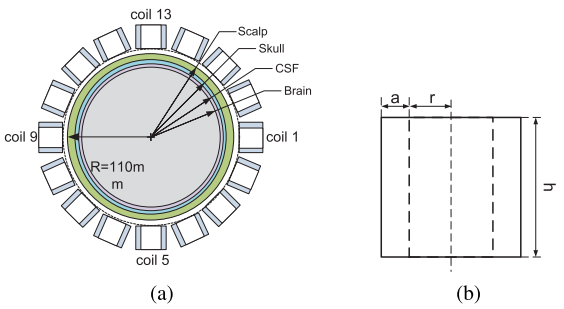

FIGURE 1. Simulation model. (a) Coils and brain model. (b) Coil structure.

The coils distribution is shown in Fig. 1(a). Along the circumference of the brain model, 16 coils evenly distribute in a clockwise direction to sense the cross sectional tissue distribution inside the brain. The coil structure is shown in Fig.1(b), where r is the inner radius, $r + a$ is the external radius, h is the height, N is the number of turns. The value of a/h is defined as the coil shape.

In the coil parameters optimization, the initial coil structure is set as follows: r is 5mm, a is 5.11mm, h is 5.11mm,

N is 100, the copper wire diameter is 0.511mm. The coil parameters and the order of the optimization include the coil radius r, coil shape a/h and the number of turns N. The later parameters optimization is based on the former optimization. r ranges from 5mm to 15mm according to the size of brain model and 16-coil structure. a/h changes into 7/15, 1, 13/8, 15/7 and 3 respectively. N changes into 64, 100, 121 and 144 respectively. As the size of brain is relatively fixed, the optimal coil structure is described in absolute dimension.

D. OPTIMIZATION CRITERION

The uniformity and intensity of sensitivity matrices affect the quality of reconstructed images [30]. The purpose of the optimization is to obtain the optimal coil structure under which the sensitivity matrix has high intensity and good uniformity. In order to quantify the intensity and uniformity, the arithmetic mean A and the coefficient of variation CV of the sensitivity matrices are calculated. In statistics, A is the measure of central tendency. The intensity of the sensitivity is evaluated as (11):

$$S_i = \sum_{m=1}^{M} S_{m,i} \tag{10}$$

$$A = \frac{1}{n}\sum_{i=1}^{n} S_i \tag{11}$$

where M is the number of combinations of exciting coils and sensing coils, S_i is the sum of the sensitivity in voxel i among all combinations, n is the quantity of voxels in the measured field. The bigger A is, the higher the sensitivity intensity is. CV is defined as the ratio of the standard deviation D to A. CV is a standardized measure of dispersion of a distribution, showing the extent of variability in relation to the mean. The uniformity of the sensing field is evaluated as (13):

$$D = \sqrt{\frac{1}{n-1}\sum_{i=1}^{n}(S_i - A)^2} \tag{12}$$

$$CV = \frac{D}{A} \tag{13}$$

The smaller CV is, the more uniform the sensitivity is. In order to unify two criteria into a consistent law, $1/CV$ is taken to measure the uniformity. In a word, the bigger A and $1/CV$ is, the better the sensitivity matrix is. Since the conductivity of biological tissues is generally low, increasing the intensity of the sensitivity is primarily concerned in the optimization of an MIT sensor array. Besides the intensity, the uniformity should also be taken into account.

E. VERIFICATION OF OPTIMIZATION

In order to verify the performance of the coil optimization, the reconstructed conductivity $\Delta\sigma_c$ is compared with the actual conductivity $\Delta\sigma_a$. The distribution of the conductivity is reconstructed by three algorithms: Landweber iteration, Newton-Raphson method and Tikhonov regularization method respectively. The factors of the algorithms are selected to have the optimal reconstructed images. After the reconstruction, $\Delta\sigma_c$ is compared to $\Delta\sigma_a$. The more similar they are, the better the sensor array is. Besides the similarity, the maximum $\Delta\sigma_c$ is also taken into account under different sensor arrays. The larger the maximum $\Delta\sigma_c$ is, the more obvious the hematoma is in the reconstructed image.

The similarity between $\Delta\sigma_c$ and $\Delta\sigma_a$ is measured by correlation coefficient C and mean-square error MSE between them:

$$C(\Delta\sigma_c, \Delta\sigma_a) = \frac{Cov(\Delta\sigma_c, \Delta\sigma_a)}{\sqrt{Var[\Delta\sigma_c] \cdot Var[\Delta\sigma_a]}}) \tag{14}$$

$$MSE = \sqrt{\frac{1}{n-1}\sum_{i=1}^{n}(\Delta\sigma_c - \Delta\sigma_a)^2} \tag{15}$$

where $Cov(\Delta\sigma_c, \Delta\sigma_a)$ is the covariance between $\Delta\sigma_c$ and $\Delta\sigma_a$, $Var[\Delta\sigma_c]$ and $Var[\Delta\sigma_a]$ are the variance of $\Delta\sigma_c$ and $\Delta\sigma_a$. In statistics, the correlation coefficient is a numerical measure of correlation, meaning a statistical relationship between two variables. The value of C reflects the correlation between $\Delta\sigma_c$ and $\Delta\sigma_a$. The larger the C is, the higher the correlation is. MSE reflects the degree of difference between $\Delta\sigma_c$ and $\Delta\sigma_a$. The smaller the MSE is, the less difference exists between them.

The maximum $\Delta\sigma_c$ is considered in the number of turns optimization. In this verification, the maximum $\Delta\sigma_c$ should be considered primarily as it varies a lot under different number of turns. The growth rates GR of the maximum $\Delta\sigma_c$ is proposed, which reflects the increment compared to 100 turns. GR is calculated as (16):

$$GR = \frac{max(\Delta\sigma_{N=n}) - max(\Delta\sigma_{N=100})}{max(\Delta\sigma_{N=100})} \tag{16}$$

where $\Delta\sigma_{N=n}$ is the conductivity change when the number of turns is n. The larger the GR is, the better the coil array is. If the optimal coil array has a better image reconstruction result than the other sensor arrays, the optimization is considered to be reasonable.

F. RESOLUTION STUDY

In the resolution study, a hematoma is set in the brain model. The hematoma center is 75mm away from the brain model center with the radius of 15mm. The object of study is peripheral hematoma as MIT has the characteristics of low central sensitivity. Based on the simulated model, the simulations are performed as follows. One coil is excited and the other coils are set as the sensing coils. Starting from coil 1, the 16 coils are sequentially excited and the voltages of the sensing coils at 1MHz and 10MHz are respectively recorded. In order to obtain the three-dimensional sensitivity matrix, voxel meshes of a cylinder containing the brain model are performed. The cylinder is divided into 17 layers from top to bottom. Each layer is divided into 256 voxels uniformly. After that, there are a total of 4352 cubes in the measured field with the side of 12mm. The vertexes of the cubes act as the mesh nodes where the electric field intensity is extracted. Then the

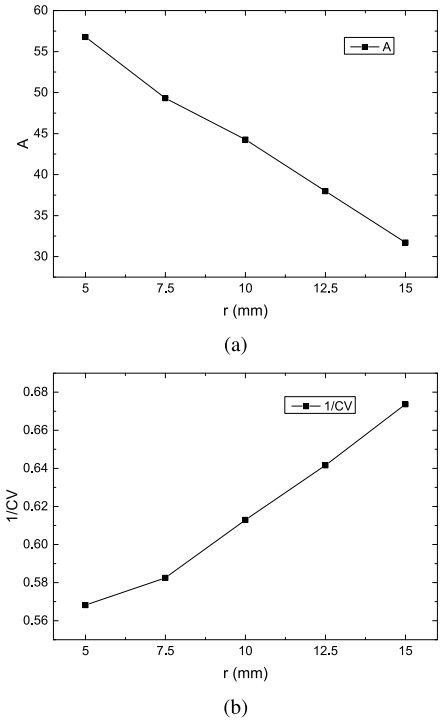

FIGURE 2. Values of A and $1/CV$ under different inner radius. (a) A. (b) $1/CV$.

three-dimensional sensitivity matrix is obtained. As for the reconstruction, 5% additive white Gaussian noise (AWGN) is added to $\Delta\Phi$ with the consideration of system noise. That is, the SNR of the system is 26dB calculated as (17):

$$SNR = 20lg\frac{\Delta\Phi}{\Delta\Phi_n}. \tag{17}$$

where $\Delta\Phi_n$ is the noise added to $\Delta\Phi$. Landweber iteration is selected as the image reconstruction algorithm after comparing the reconstructed images of three algorithms. In the study of resolution, a threshold of the $\Delta\sigma_c$ is selected. The conductivity change below this threshold is set to zero to improve the quality of reconstructed images.

Based on the optimal coil structure, the conductivity resolution CR and spatial resolution SR of the intracranial hematoma detected by dual frequency-difference MIT is studied. CR is the minimum conductivity change that can be detected. SR is defined as the ratio of hematoma radius to brain model radius:

$$SR = \frac{R_h}{R_b} \cdot 100\% \tag{18}$$

where R_h is the radius of the hematoma, R_b is the radius of the brain model.

III. RESULTS AND ANALYSIS

A. COIL PARAMETERS OPTIMIZATION

1) COILS INNER RADIUS

The optimization of coil inner radius is necessary as the inner radius affects the distribution of the magnetic field. The larger the inner radius is, the more uniform the distribution of the magnetic field intensity is. But if the inner radius is too large, interference occurs between adjacent coils [11]. Therefore, there should be an optimal coil inner radius.

In this simulation, r changes into 5mm, 7.5mm, 10mm, 12.5mm and 15mm respectively while a, h, and N are unchanged. Corresponding to the change of r, the external radius changes into 10.11mm, 12.61mm, 15.11mm, 17.61mm and 20.11mm respectively. Under different inner radius, the value of A and $1/CV$ is shown in Fig. 2. With the increment of the inner radius, the value of A decreases while $1/CV$ increases. That is, the intensity of the sensitivity matrix decreases and the uniformity of the sensitivity matrix increases. After considering the tradeoff between A and $1/CV$, 7.5mm is chosen as the optimal inner radius. Under this condition, A is big enough while $1/CV$ is not too small. That is, the intensity of the sensitivity matrix is large enough and the uniformity is not too poor when r is 7.5mm.

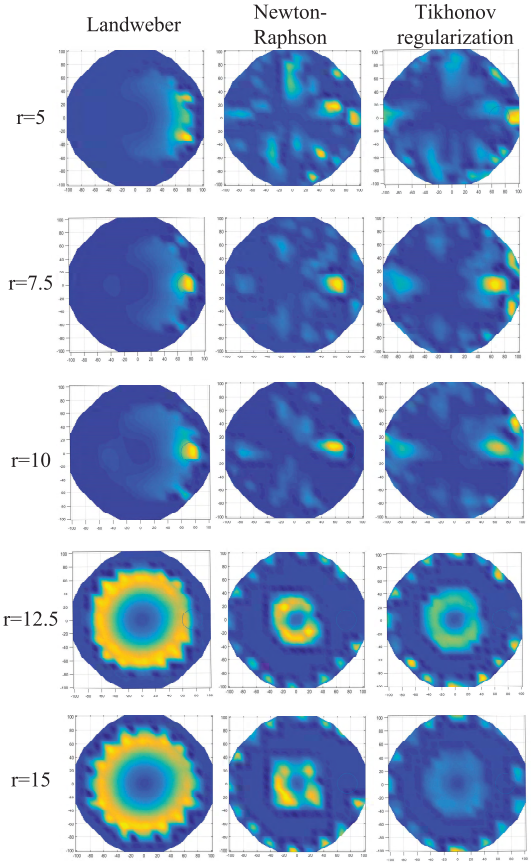

FIGURE 3. Reconstructed images under different inner radius.

In order to verify the optimization, $\Delta\sigma_c$ is compared to $\Delta\sigma_a$. The reconstructed images of $\Delta\sigma_c$ under different inner radii are shown in Fig.3. The value of C between $\Delta\sigma_c$ and $\Delta\sigma_a$ is shown in Fig. 4(a). The larger C is, the more similar $\Delta\sigma_c$ and $\Delta\sigma_a$ are, therefore the better the reconstructed image is. The results with negative C represent a negative correlation. With the increment of the inner radius, the value of C firstly increases and then decreases. When the inner radius is

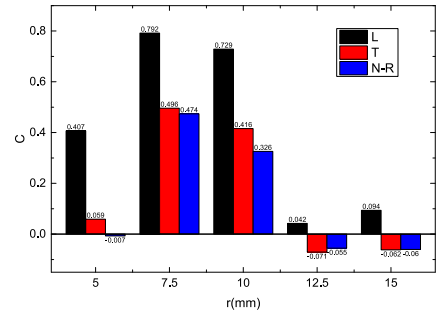

(a)

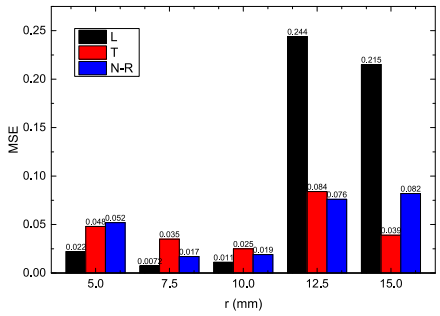

(b)

FIGURE 4. Values of C and MSE under different inner radius. (L, T and N-R respectively represent Landweber iteration, Tikhonov regularization method and Newton-Raphson method.) (a) C. (b) MSE.

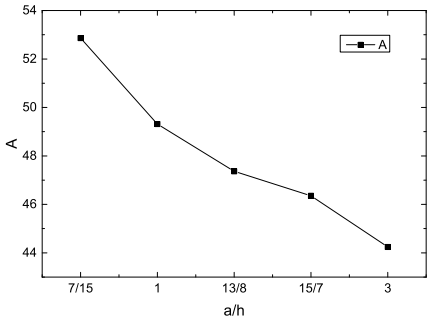

(a)

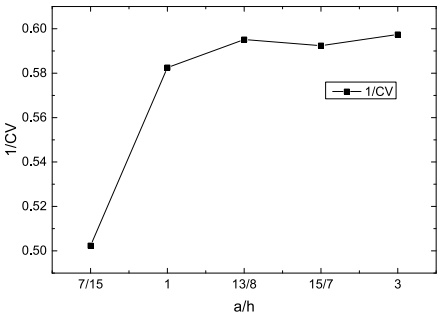

(b)

FIGURE 5. Values of A and $1/CV$ under different coil shapes. (a) A. (b) $1/CV$.

7.5mm, it has the biggest similarity among three algorithms. The MSE between $\Delta\sigma_c$ and $\Delta\sigma_a$ is shown in Fig. 4(b). The larger the MSE is, the worse the reconstructed image is. With the increment of the inner radius, the value of MSE firstly decreases and then increases. The coil with 7.5mm inner radius has the smallest value of MSE among the algorithms of Newton-Raphson method and Landweber iteration. Considering both C and MSE, 7.5mm is verified to be the optimal coil inner radius.

TABLE 2. Dimensions of and under different coil shapes.

a/h	7/15	1	13/8	15/7	3
a(mm)	3.577	5.110	6.643	7.665	9.198
h(mm)	7.665	5.110	4.088	3.577	3.066

2) COILS SHAPE

The influence of different coil shapes on sensitivity matrices is studied. Based on the optimization of the coils inner radius, r is set to 7.5mm. a/h changes as shown in Table 2. The values of A and $1/CV$ are shown in Fig.5 under different coil shapes. With the increment of a/h, the value of A gradually decreases while the value of $1/CV$ quickly grows at first and then tends to be steady. The turning point is the place where a/h is equal to 1. Taking two criteria into consideration, 1 is chosen as the optimal value of a/h. Under this condition, the values of A and $1/CV$ are both large enough. That is, the intensity is large enough and the uniformity is good.

After the coil shape optimization, $\Delta\sigma_c$ is compared to $\Delta\sigma_a$ for verification. Fig. 7(a) is the C between $\Delta\sigma_c$ and $\Delta\sigma_a$. When a/h is 7/15, the value of C is much smaller than that of the other shapes. The results with negative C represent a negative correlation. When a/h is greater than or equal to 1, the value of C tends to be similar. The biggest C is obtained when a/h is 1. Under this condition, it has the biggest similarity among three algorithms. The MSE between $\Delta\sigma_c$ and $\Delta\sigma_a$ is shown in Fig. 7(b). When a/h is 7/15, the value of MSE is much larger than that of the other shapes. When a/h is greater than or equal to 1, the values are similar. The smallest value of MSE is acquired when a/h is 1 among the algorithms of Newton-Raphson method and Landweber iteration. Considering both C and MSE, 1 is verified to be the optimal value of a/h.

3) NUMBER OF TURNS

In the number of turns optimization, N changes into 64, 100, 121, 144 respectively. r is 7.5mm and a/h is 1 based on the optimization of the coil inner radius and shape. Corresponding to the change of N, a, and h are 4.088, 5.110, 5.621, 6.132 respectively while r is unchanged. Fig. 8 shows the values of A and $1/CV$ under different number of turns. When N is 121, the intensity of sensitivity is larger than that of the other coils. Therefore, 121 is selected as the optimal number of turns.

Under different number of turns, the reconstructed images are shown in Fig. 9. The values of GR under different number of turns are extracted and shown in Fig. 10. The coil with 121 turns has the biggest value of GR. Namely, when the

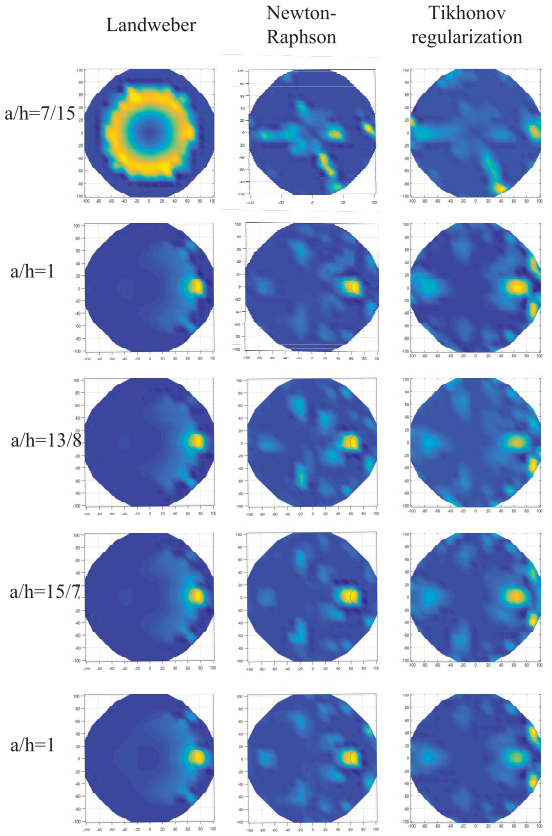

FIGURE 6. Reconstructed images under different shapes.

conductivity change is small, the coils with 121 turns can detect it more easily. Therefore, 121 is verified to be the optimal number of turns.

After the coil parameters optimization, the optimal coil structure is shown in Fig. 11, the parameters are set as follows: r is 7.5mm, a/h is 1, a and h are both 5.621mm, N is 121.

4) DISCUSSION

In terms of the uniformity of the sensitivity matrix, a coil that has a large inner radius and a flat shape is preferable. However, the intensity of the sensitivity matrix varies oppositely. Both the uniformity and the intensity of the sensitivity matrix need to be balanced in the coil structure optimization. Since the conductivity of different biological tissues varies little, increasing the intensity of the sensitivity is primarily concerned in the optimization of the sensor array in an MIT system. Besides the intensity, the uniformity is the second factor to consider.

In the simulations of the inner radius optimization, the results in Fig. 2 show that the inner radius has an obvious impact on the intensity and uniformity of the sensitivity matrix. The values of A and $1/CV$ change in an approximately linear law with different inner radii. The inner radius of 7.5mm is chosen as the optimal value as the intensity of the sensitivity matrix is large while the uniformity is not too low.

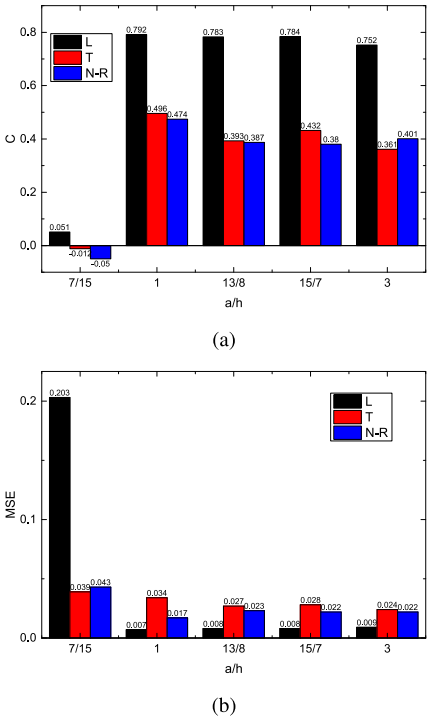

FIGURE 7. Values of C and MSE under different coil shapes. (L, T and N-R respectively represent Landweber iteration, Tikhonov regularization method and Newton-Raphson method.) (a) A. (b) $1/CV$.

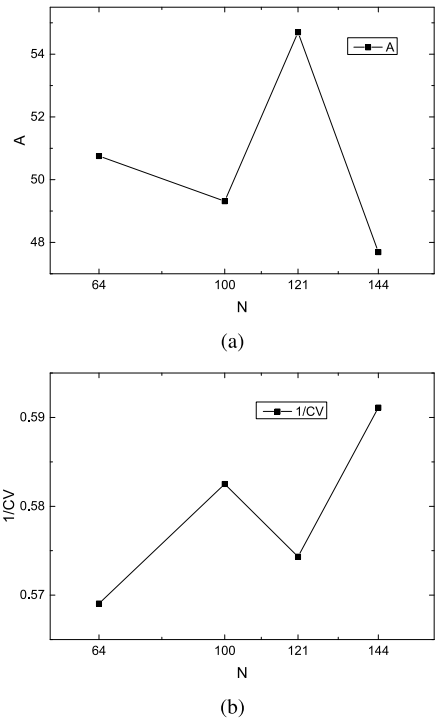

FIGURE 8. Values of A and $1/CV$ under different number of turns. (a) A. (b) $1/CV$.

In the simulations of the coil shapes optimization, when a/h is smaller than 1, the sensitivity matrix has a bad character with low intensity and uniformity. When a/h is greater than or equal to 1, the character of the sensitivity matrix is

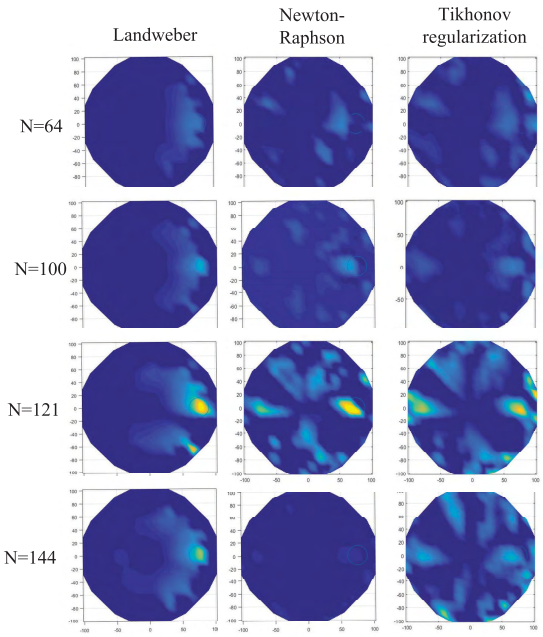

FIGURE 9. Reconstructed images under different number of turns.

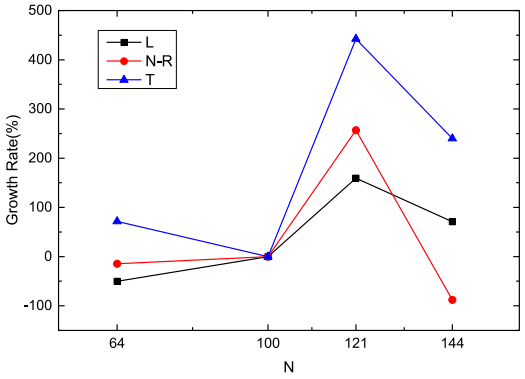

FIGURE 10. The growth rate under different number of turns. (L, N-R and T respectively represent Landweber iteration, Newton-Raphson method and Tikhonov regularization method.)

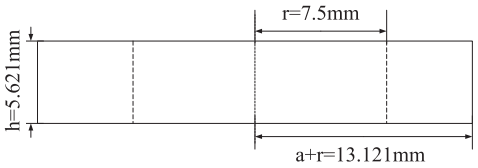

FIGURE 11. The dimension of the optimal coils.

better than the former. The criteria of the sensitivity matrix under different shapes vary little. Therefore, the coil shapes have a smaller impact on the character of the sensitivity matrix when a is larger than or equal to h. After the optimization of coil shapes, 1 is the optimal value of a/h.

As for the number of turns optimization, the coil with more turns can produce a stronger magnetic field strength. However, it will also have a larger impedance, which will place a great demand on the load capacity of the excitation. Therefore, the number of turns have an optimal value. After the optimization, the optimal number of turns is 121.

B. RESOLUTION ANALYSIS

The location of the hematoma is shown in Fig. 12, whose center is 75mm away from the brain model center with the radius of 15mm.

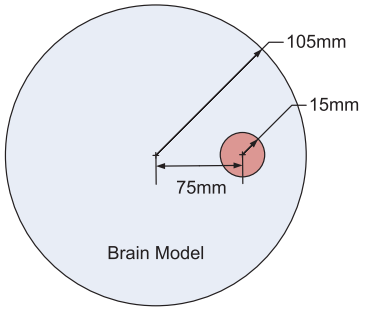

FIGURE 12. Location of hematoma simulation model.

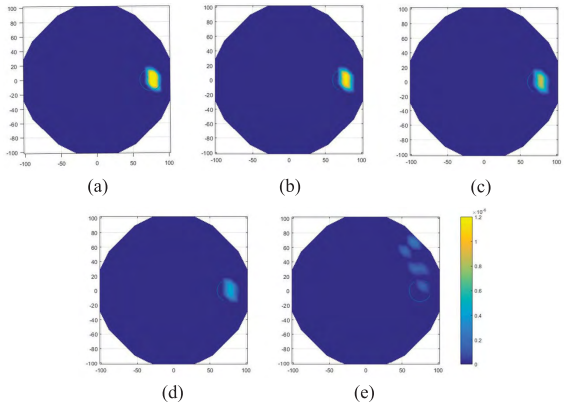

FIGURE 13. Reconstructed images of hematomas with different conductivity changes. (a) 1.82S/m. (b) 1.57S/m. (c) 1.32S/m. (d) 1.07S/m. (e) 0.92S/m.

1) CONDUCTIVITY RESOLUTION

In order to study the conductivity resolution, different conductivity changes are set as follows: 1 S/m, 0.75 S/m, 0.5 S/m, 0.25 S/m and 0.1S/m respectively. That is, σ_{f1} is 0.82S/m, σ_{f2} is 1.82 S/m, 1.57 S/m, 1.32 S/m, 1.07 S/m and 0.92S/m respectively. These values are within the range of actual biological tissues conductivity. As shown in Fig. 13, the images are reconstructed with 26dB noise. When $\Delta\sigma$ is 1 S/m or 0.75S/m, the hematoma is clearly in the figure. With the decrease of the $\Delta\sigma$, the hematoma is less obvious. When the $\Delta\sigma$ is 0.1S/m, the specific position and size of the hematoma are unable to be determined due to the effect of added noise. The hematoma is submerged in the artifacts if the signals are too weak. In this simulation, the conductivity resolution is 0.25S/m.

2) SPATIAL RESOLUTION

Based on the optimal coil structure, the spatial resolution is also studied. The radius of the hematoma is set to 15mm,

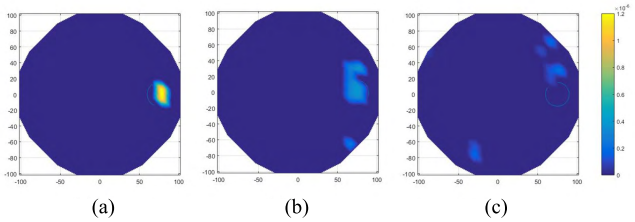

FIGURE 14. Reconstructed images of hematomas with different sizes. (a) 15mm. (b) 13mm. (c) 11mm.

13mm, 11mm respectively, that is, *SR* is 14.29%, 12.38% and 10.48% respectively. As Fig. 13(b) is of high quality, the change of conductivity is set to 0.75S/m. As shown in Fig. 11, the images of different hematoma radii are reconstructed with 26dB noise. When the radius is 15mm, the hematoma is clearly reconstructed. When the radius is 13mm, the reconstructed image shows the possible bleeding area, which is larger than the actual distribution due to impact of noise. When the radius is 11mm, the hematoma is unable to see from the reconstructed image. From the results it can be seen that the radius of the hematoma has a huge impact on the detection. If the hematoma is too small, the reconstructed image of the hematoma will be submerged in the artifacts. In this simulation, the spatial resolution is 12.38% with SNR 26dB.

IV. CONCLUSIONS

In order to enhance the resolution of dual frequency-difference MIT, the sensor array is optimized based on two criteria. The resolution of the optimal sensor array is studied with added noise. The coil parameters optimization is simulated from three aspects: coil inner radius, shapes and number of turns. The intensity and uniformity of sensitivity matrices are extracted as the criteria. After the optimization, the optimal coil structure is obtained: r is 7.5mm, a/h is 1, a and h are both 5.621mm, N is 121. Based on the three-dimensional brain model with a hematoma, the images are reconstructed with the optimal sensor array. The conductivity resolution and the spatial resolution are studied respectively. The results show that the optimal sensor array can achieve the conductivity resolution of 0.25S/m and the spatial resolution of 12.38%. This study will lay the foundation for the design of sensor array in an MIT system.

REFERENCES

[1] R. F. Keep, Y. Hua, and G. Xi, "Intracerebral haemorrhage: Mechanisms of injury and therapeutic targets," *Lancet Neurol.*, vol. 11, no. 8, pp. 720–731, 2012.
[2] Y. Wang, Y. Shao, Z. Gui, Q. Zhang, L. Yao, and Y. Liu, "A novel fractional-order differentiation model for low-dose CT image processing," *IEEE Access*, vol. 4, pp. 8487–8499, 2016.
[3] W. Pan *et al.*, "Detection of cerebral hemorrhage in rabbits by time-difference magnetic inductive phase shift spectroscopy," *PLoS ONE*, vol. 10, no. 5, p. e0128127, 2015.
[4] L. Wang, R.-G. Liu, W. Zhou, and X.-Z. Dong, "Research progress of magnetic induction tomography system and experimental results," *Chin. Med. Equip. J.*, vol. 34, no. 2, pp. 85–88, 2013.
[5] Z. Xu, Y. Jiang, B. Wang, Z. Huang, H. Ji, and H. Li, "Sensitivity distribution of CCERT sensor under different excitation patterns," *IEEE Access*, vol. 5, pp. 14830–14836, 2017.
[6] R. Liu, Y. Li, F. Fu, F. You, X. Shi, and X. Dong, "Time-difference imaging of magnetic induction tomography in a three-layer brain physical phantom," *Meas. Sci. Technol.*, vol. 25, no. 6, p. 065402, 2014.
[7] D. Gürsoy and H. Scharfetter, "Feasibility of lung imaging using magnetic induction tomography," in *Proc. World Congr. Med. Phys. Biomed. Eng.* Munich, Germany: Springer, 2009.
[8] C. Deans, L. Marmugi, S. Hussain, and F. Renzoni, "Optical atomic magnetometry for magnetic induction tomography of the heart," *Proc. SPIE*, vol. 9900, Apr. 2016, Art. no. 99000F, doi: 10.1117/12.2227538.
[9] A. Morris, H. Griffiths, and W. Gough, "A numerical model for magnetic induction tomographic measurements in biological tissues," *Physiol. Meas.*, vol. 22, no. 1, p. 113, 2001.
[10] L. Wang and A. M. Al-Jumaily, "Imaging of lung structure using holographic electromagnetic induction," *IEEE Access*, vol. 5, pp. 20313–20318, 2017.
[11] H.-Y. Wei and M. Soleimani, "Electromagnetic tomography for medical and industrial applications: Challenges and opportunities," *Proc. IEEE*, vol. 101, no. 3, pp. 559–565, Mar. 2013.
[12] X. Chen and T. Ding, "Flexible eddy current sensor array for proximity sensing," *Sens. Actuators A, Phys.*, vol. 135, no. 1, pp. 126–130, 2007.
[13] A. J. Peyton *et al.*, "An overview of electromagnetic inductance tomography: Description of three different systems," *Meas. Sci. Technol.*, vol. 7, no. 3, p. 261, 1996.
[14] H. Scharfetter, H. K. Lackner, and J. Rosell, "Magnetic induction tomography: Hardware for multi-frequency measurements in biological tissues," *Physiol. Meas.*, vol. 22, no. 1, pp. 131–146, 2001.
[15] D. Gürsoy and H. Scharfetter, "The effect of receiver coil orientations on the imaging performance of magnetic induction tomography," *Meas. Sci. Technol.*, vol. 20, no. 10, p. 105505, 2009.
[16] Y. Lv, X. Wang, and J. Jin, "Simulation study of coils sensor preferences in magnetic induction tomography," in *Proc. 8th World Congr. Intell. Control Automat.*, Jul. 2010, pp. 5367–5370.
[17] K. Xu, W. Yin, and H. Wang, "EMT Sensor optimization based on analysis of sensitivity matrix," (in Chinese), *J. Test Meas. Technol.*, vol. 25, no. 1, pp. 72–77, 2011, doi: 10.3969/j.issn.1671-7449.2011.01.013.
[18] H. Griffiths, "Magnetic induction tomography," *Meas. Sci. Technol.*, vol. 12, no. 8, pp. 1126–1131, 2001.
[19] N. G. Gencer and M. N. Tek, "Electrical conductivity imaging via contactless measurements," *IEEE Trans. Med. Imag.*, vol. 18, no. 7, pp. 617–627, Jul. 1999.
[20] A. Korjenevsky, V. Cherepenin, and S. Sapetsky, "Magnetic induction tomography: Experimental realization," *Physiol. Meas.*, vol. 21, no. 1, pp. 89–94, 2000.
[21] H. Griffiths, W. R. Stewart, and W. Gough, "Magnetic induction tomography: A measuring system for biological tissues," *Ann. New York Acad. Sci.*, vol. 873, no. 1, pp. 335–345, 1999.
[22] M. S. B. Mansor *et al.*, "Magnetic induction tomography: A brief review," *Jurnal Teknologi Sci. Eng.*, vol. 73, no. 3, pp. 91–95, 2015.
[23] Z. Xiao, C. Tan, and F. Dong, "Multi-frequency difference method for intracranial hemorrhage detection by magnetic induction tomography," *Physiol. Meas.*, vol. 39, no. 5, p. 055006, 2018.
[24] M. Zolgharni, H. Griffiths, and P. D. Ledger, "Frequency-difference MIT imaging of cerebral haemorrhage with a hemispherical coil array: Numerical modelling," *Physiol. Meas.*, vol. 31, no. 8, p. S111, 2010.
[25] Z. Xu, W. He, C. He, and Z. Zhang, "Analytical method for the potential distribution of head sphere model under the stimulation of point current source," *J. Biomed. Eng.*, vol. 25, no. 4, pp. 779–784, 2008.
[26] K. Hollaus, C. Magele, R. Merwa, and H. Scharfetter, "Fast calculation of the sensitivity matrix in magnetic induction tomography by tetrahedral edge finite elements and the reciprocity theorem," *Physiol. Meas.*, vol. 25, no. 1, pp. 159–168, 2004.
[27] C. Ktistis, D. W. Armitage, and A. J. Peyton, "Calculation of the forward problem for absolute image reconstruction in MIT," *Physiol. Meas.*, vol. 29, no. 6, pp. S455–S464, 2008.
[28] R. Merwa, K. Hollaus, P. Brunner, and H. Scharfetter, "Solution of the inverse problem of magnetic induction tomography (MIT)," *Physiol. Meas.*, vol. 26, no. 2, p. S241, 2005.
[29] H. Buchner, T. D. Waberski, M. Fuchs, H.-A. Wischmann, M. Wagner, and R. Drenckhahn, "Comparison of realistically shaped boundary-element and spherical head models in source localization of early somatosensory evoked potentials," *Brain Topogr.*, vol. 8, no. 2, pp. 137–143, 1995.
[30] C. Wang, J. Zhang, F. Li, Z. Cui, and C. Xu, "Design of a non-magnetic shielded and integrated electromagnetic tomography system," *Meas. Sci. Technol.*, vol. 22, no. 10, p. 104007, 2011.

CHAO TAN (M'09–SM'15) received the B.S., M.S. and Ph.D. degrees in control science and engineering from Tianjin University, Tianjin, China, in 2003, 2006, and 2009, respectively. Since 2009, he has been a Lecturer and then promoted to an Associate Professor with the School of Electrical and Information Engineering, Tianjin University.

His research interests include process parameter detection and control systems, biomedical imaging, multiphase flow measurement and instrumentation, industrial process tomography, and multisensor/data fusion.

YIRAN WU received the B.S. degree in control science and engineering from Tianjin University, Tianjin, China, in 2017, where she is currently pursuing the M.S. degree in control science and engineering. Her research interests include magnetic inductance tomography system design and optimization.

ZHILI XIAO received the B.S. degree in control science and engineering from the Hebei University of Technology in 2013. She is currently pursuing the Ph.D. degree in control science and engineering with Tianjin University. Her research interests include magnetic inductance tomography image reconstruction, brain hemorrhage imaging, and sensor optimization.

FENG DONG (M'03–SM'06) received the B.S., M.S., and Ph.D. degrees in control science and engineering from Tianjin University, Tianjin, China, in 1988, 1996, and 2002, respectively. He is currently a Professor with the School of Electrical and Information Engineering, Tianjin University, and the Director of the Tianjin Key Laboratory of Process Measurement and Control, Tianjin University.

He is currently the Vice President of the International Society of Industrial Process Tomography. His research interests include process parameter detection and control system, industrial process tomography, multiphase flow measurement, and intelligent information processing.